Origin of preferential sputtering in *a*-SiO_2 during ion beam synthesis of nanocrystals

M. J. Beck[1,*] and S. T. Pantelides[1,2]
[1]*Department of Physics and Astronomy, Vanderbilt University, Nashville, Tennessee 37235, USA*
[2]*Solid State Division, Oak Ridge National Laboratory, Oak Ridge, Tennessee 37831, USA*
(Received 29 September 2008; revised manuscript received 10 December 2008; published 21 January 2009)

Ion implantation into *a*-SiO_2 leads to the self-assembly of nanocrystal arrays having application in optical and nonvolatile memory devices. It was recently noted that nanocrystal nucleation occurs in oxide regions exhibiting variations in oxygen concentration resulting from preferential sputtering. Here we report quantum-mechanical calculations that probe the atomic-scale dynamics following ion-induced low-energy recoils and show that preferential sputtering does not result directly from short-time collisional processes. These processes do, however, result in a population of loosely bound oxygen atoms connected to the amorphous network by a single Si-O bond. Thus, the well-known diffusion and relaxation processes that control stable defect formation at long times following recoil events lead to variations in O concentration in damaged regions.

DOI: 10.1103/PhysRevB.79.033203 PACS number(s): 61.80.Jh, 61.82.Ms

Ion beam modification of surface and bulk material properties continues to generate significant interest as an inexpensive method for producing nanoscale features in electronic and optical devices. Recently, ion implantation of *a*-SiO_2 with group-IV or metallic ions followed by annealing has been shown to result in the self-assembly of electrically and/or optically active nanocrystals within the *a*-SiO_2 matrix.[1,2] Studies have highlighted the importance of incident ion energy and flux,[3–6] as well as annealing time, temperature, and atmosphere,[6,7] as factors controlling the depth, size, uniformity, optical, and electronic properties of nanocrystal arrays in *a*-SiO_2. Optimizing processing parameters for controlled fabrication of uniform nanocrystal arrays depends on the development of a detailed atomic-scale understanding connecting implant conditions to nanocrystal nucleation and growth.

A recent study[8] probing the relationship between implant conditions and resulting nanocrystal properties has shown that stoichiometric imbalances involving O-rich and O-poor regions appear in *a*-SiO_2 during implantation. These variations in relative Si and O concentration—as well as the ion-induced nanocrystals themselves—occur in the incident ion end-of-range region where ion-induced effects are dominated by low-energy ($\ll 1$ keV) atomic recoils. Other studies[9–11] have previously suggested that similar variations in O concentration play a role in controlling nanocrystal nucleation and growth. The appearance of concentration variations in implanted *a*-SiO_2 has been attributed to preferential O scattering or sputtering.[8] Ion-induced scattering occurs when atomic recoils result in mass transport within the target bulk, while sputtering is the removal of atoms resulting from near-surface scattering (e.g., for low-energy implants having shallow end-of-range regions). Preferential O sputtering has been observed in the context of oxide decomposition during ion implantation[12–14] and electron or ion beam nanopore formation.[15,16] To date, the relative roles of ballistic cascade effects and thermal diffusion effects in preferential sputtering have not been fully elucidated. Determining which class of mechanisms controls preferential sputtering will provide insight into the optimization of implant parameters for ion beam assisted nucleation of nanocrystal arrays.

Molecular dynamics (MD) simulations have been widely applied to study the dynamic atomic-scale processes occurring during ion implantation and sputtering.[17,18] Using various models for interatomic interactions, MD methods have allowed many-atom simulations of the atomic motions in systems during and/or following ion-induced collision cascades, including in SiO_2.[19,20] Dynamical calculations based on density-functional theory and employing highly accurate quantum-mechanical descriptions of the interatomic forces have been previously conducted to determine the threshold displacement energy in SiC (Refs. 21 and 22) and crystalline Si.[23] Similar calculations have also highlighted the role of complex, many-body, bond-breaking, and bond-forming events in controlling collisional processes in ion-induced cascades in bulk Si.[24] Overall, it has been generally acknowledged that diffusion and relaxation processing following recoil events dominate the process of stable defect formation.[17,19,21,22]

In this Brief Report we report results of first-principles density-functional calculations of the dynamics of low-energy recoils in *a*-SiO_2 designed to test the alternative hypothesis that direct collisional processes alone can result in the preferential O sputtering previously reported in *a*-SiO_2. We show that for low-energy (100 eV) Si and O recoils, recoil energy dissipation involves tens of atoms and leads to the formation of numerous network defects, analogous to the amorphous pocket formation reported elsewhere for medium energy (~ 1 keV) recoils.[17] We find that for times up to the end of direct collisional processes and the beginning of thermally activated relaxation and diffusion processes (<100 fs), no stoichiometric imbalances appear. However, the nature of the network defects generated by low-energy recoils in *a*-SiO_2 contributes to the appearance of concentration variations during diffusion, supporting the conclusion that preferential sputtering and resulting changes in relative Si and O concentration are a product of previously studied long-time diffusion and relaxation processes. Finally we highlight that the high density of Si dangling bonds generated in the recoil region represents highly reactive centers for the nucleation of nanocrystals.

The dynamics of low-energy Si and O recoils were modeled in 192 atom periodic *a*-SiO_2 supercells generated using a Monte Carlo bond switching method.[25,26] In separate simu-

 ©2009 The American Physical Society

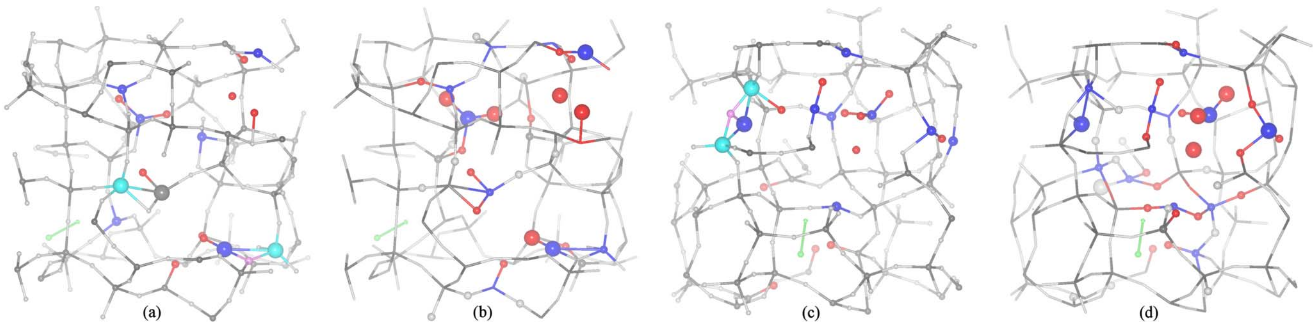

FIG. 1. (Color online) a-SiO_2 cells after 100 eV O [(a) and (b)] and Si [(c) and (d)] recoils. [(a) and (c)] Si and O network defects: dangling bonds (dark balls), overcoordinated atoms (light balls), and self-bonded atoms (large balls). [(b) and (d)] Recoil energy dissipation and displacements: "hot" Si and O atoms (dark balls), atoms displaced ≥ 1.17 Å and atoms displaced ≥ 0.2 Å but < 1.17 Å (large and small balls). The recoil atom initial position and direction is indicated with a green ball and vector. See text for details.

lations, recoil atoms of each species were assigned initial velocities corresponding to a kinetic energy of $E_r = 100$ eV to represent the low-energy recoils which dominate in the end-of-range region. Five recoil directions for each species were selected, sampling a range of recoil paths in the a-SiO_2 network. Interatomic forces were calculated using density-functional theory, the local-density approximation,[27] ultrasoft pseudopotentials,[28] and a plane-wave basis with an energy cutoff of 540 eV. Eigenvalues were calculated at the reciprocal space point $(\frac{1}{4}, \frac{1}{4}, \frac{1}{4})$. Atomic motions were calculated according to Newton's equations and the calculated forces for time steps of 0.38 (Si recoils) and 0.29 (O recoils) fs. The time steps were chosen so no atom traveled >0.1 Å in any time step. No thermostat is applied during the calculations; thus the sum of the kinetic energy and potential energy of the system is constant. The use of pseudopotentials to describe the ion cores is appropriate for the kinetic energies considered here as determined based on test calculations of binary collisions, and on the results of an extensive previous study.[29]

The results of a recent study[8] show that O atoms are preferentially scattered *along* the direction of the incident beam during implantation. This leads to an O-rich region just beyond the incident ion end of range. Studies of oxide decomposition during ion irradiation find similar O-rich and O-poor regions, or, simply, that O is preferentially removed from the implanted region.[12–14] In either case, species selectivity leading to relative variations in target concentration corresponds to either (i) a preferential dissipation of recoil energy to O atoms during direct collisional processes or (ii) to an enhanced outdiffusion of O on longer time scales. To isolate and study process (i), that is, the direct collisional effects of atomic recoils in a-SiO_2, we focus on the state of the system during the initial 58 and 76 fs after O or Si recoils, respectively. At longer times the recoil energy is widely distributed within the target, and further dynamics are governed by relaxation and thermal diffusion processes. The difference between the simulation times leading up to the crossover to thermal processes for O and Si recoils arises because the ion-target collisions that dissipate ion energy to the target occur within a shorter time window for the lower mass, and therefore faster moving ($v \propto \sqrt{E_r/m}$), O ions. In addition, the crossover times employed here are consistent with the existence, reported in a previous study,[22] of a "point of no return" for ballistic damage formation occurring ~ 70 fs after 20 eV recoils. For $v \propto \sqrt{E_r/m}$, the comparable time for 100 eV recoils (as studied here) is ~ 30 fs.

Figure 1 shows a-SiO_2 structures following the direct collisional phase of system evolution after representative O [(a) and (b)] and Si [(c) and (d)] 100 eV recoils. Panels (a) and (c) highlight the dynamic network defects formed during each recoil event. These defects are not necessarily stable, final-state defects that will survive long-time relaxation and diffusive processes. Rather, these defects represent the dynamic disorder induced in the network structure of a-SiO_2 as a direct result of the ballistic collision cascade. Defects are identified by examining the nearest-neighbor configurations of each atom. Bonds between neighbors are taken to be present when neighbor distances are <1.6, 1.9, and 2.6 Å for O-O, Si-O, and Si-Si neighbors, respectively, and are shown with sticks in Fig. 1. Undercoordinated Si and O atoms are considered to have one or more dangling bonds and are shown as dark balls (blue and red, respectively, in online version). Light balls (light blue and pink in online version) are overcoordinated Si and O atoms, and large balls indicate atoms with self-bonds (e.g., Si-Si or O-O). Si and O atoms not flagged as defect atoms are located at the intersections of dark gray or light gray sticks, respectively. The green ball and vector indicates the initial position and recoil direction of the recoil atom.

Figures 1(a) and 1(c) show that a high density of dynamic network defects is generated during the collision cascade. These defects appear in a region ~ 10 Å in diameter and centered ~ 10 Å from the recoil atom's initial position. This is analogous to the amorphous pocket formation described elsewhere following recoils in crystals (see, e.g., Ref. 17). The average number of each type of defect present at the end of the ballistic collisional phase is shown in Fig. 2. Error bars are the standard deviation of the number of defects among different recoil directions. Dangling bonds are the primary defects produced during the collision cascade following low-energy recoils in a-SiO_2. The majority of defect atoms is undercoordinated or overcoordinated by one bond, and, roughly defining a minimum volume sphere containing all defects, more than half the atoms in the sphere are defect atoms. After correcting for the number of dangling bonds associated with the recoil atom alone (four of each species

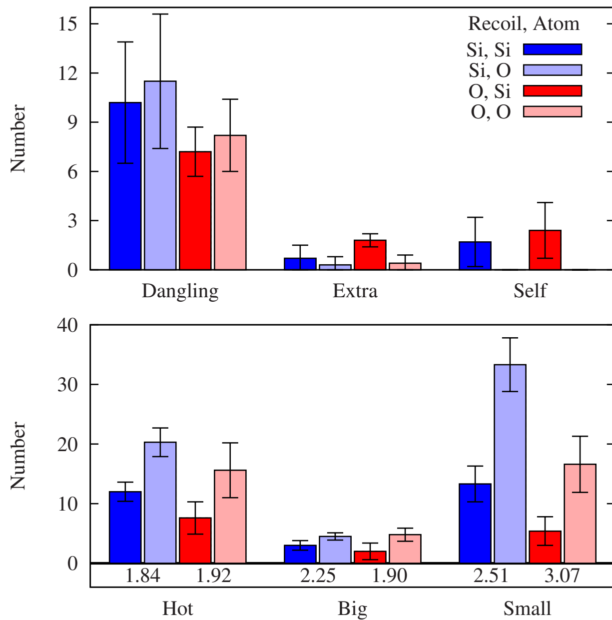

FIG. 2. (Color online) (top) Average number of atoms with dangling bonds, extra bonds, and self-bonds. (bottom) Average number and O:Si ratio of hot atoms, and atoms with large (≥1.17 Å) and small (≥0.2 Å but <1.17 Å) displacements. Bar colors indicate recoil species, and bold or light bars indicate defect/atom species. See text for details.

for a Si recoil, and two each for an O), Si recoils produced ∼20% more dangling bonds than O recoils, while O recoils produced slightly more overcoordinated and self-bonded atoms. As all recoils had the same initial kinetic energy, these variations are driven by recoil atom mass differences and the species dependence of atomic interactions.

Returning to Fig. 1, panels (b) and (d) highlight the overall dissipation of recoil energy in the same a-SiO_2 cells presented in panels (a) and (c). Analogous to the melting temperature in crystals, the glass transition temperature in a-SiO_2 ($T_g > 1200$ K) (Ref. 30) is a reference for identifying atoms with sufficient kinetic energy to have a high probability of athermally breaking bonds and moving long distances. From Boltzmann statistics, the average kinetic energy of a particle in thermal equilibrium is $\frac{3}{2}kT$. For Si or O atoms in a-SiO_2 at $T = T_g \approx 1200$ K this is 0.22 eV. We refer to atoms with kinetic energy >0.22 eV as "hot" atoms and indicate them with blue (Si) or red (O) balls in Figs. 1(b) and 1(d). Large and small balls indicate atoms displaced >1.2 and >0.2 Å from their original positions. It should be noted that the transition from the ballistic collisional phase to the thermally driven diffusion and relaxation phase of ion-induced effects is characterized, in part, by a maximum in the number of hot atoms. For times beyond this transition recoil energy is dissipated among an increasingly large number of atoms, and fewer individual atoms possess sufficient kinetic energy to athermally break bonds. Hence, thermal processes dominate ballistic processes.

The bottom panel of Fig. 2 shows the average number of hot and displaced atoms at the end of the direct collisional phase following Si and O recoils. Colors and error bars are as above. The O:Si ratio for each category of atoms is indicated below the histogram bars. The O:Si ratio for hot atoms and those displaced >1.2 Å have been corrected by adjusting for the recoil atom (which is included in the count of hot and >1.2 Å displaced atoms for all recoils). Recoil energy is dissipated to a total of ∼30 Si and O atoms, all roughly within the defected atom sphere described above. Both hot atoms and atoms displaced >1.2 Å occur with an O:Si ratio of ≈2. This corresponds to the a-SiO_2 stoichiometry, and indicates that no preferential scattering of O has occurred.

The degree of preferential scattering can be quantified by considering the net relative displacement of all O and Si atoms in each cell. Projected along the recoil direction, and correcting for the 2:1 stoichiometry of a-SiO_2, half the total displacement of all O atoms minus the total displacement of all Si atoms gives the recoil-induced separation between the O and Si centers of mass. As defined, a positive net relative displacement resulting from direct collisional processes corresponds to a preferential ballistic scattering of O, and a contribution to supersaturations of O beyond an incident ions end of range. For both the Si and O recoils studied here, we find net relative displacements on the order of ±1 Å, with an average net relative displacement of −0.9 Å. This seems to indicate that during the ballistic collisional phase preferential Si scattering occurs. In practice, though, net relative displacements of ∼±1 Å do not result in observable concentration variations, and thus the present results demonstrate that no meaningful preferential sputtering occurs during the collisional phase. Therefore, experimentally observed preferential sputtering of O leading to nanometer-scale variations in relative concentration and/or the removal of O from nanometer-scale target layers are the result of thermal, diffusion-related processes occurring on annealing timescales following a recoil event.

A diffusion-mediated origin for the observed concentration variations and stoichiometric imbalances in ion-irradiated a-SiO_2 requires that O outdiffusion from ion-modified target regions dominates Si outdiffusion. Support for this is found in the >2 O:Si ratio of atoms with small displacements. Small displacements are indicative of atoms that are unable to athermally (ballistically) break their bonds, but that, over annealing time scales, will exhibit significant thermal vibrations. In addition, while O atoms with dangling bonds are held to the network by at most one additional bond, Si atoms with dangling bonds are pinned to the network by (as generally observed here) three additional bonds. Combined with the high diffusivity of O in a-SiO_2,[31] the present results provide evidence for increased O outdiffusion from damaged regions—a process whose role in nanocrystal formation has been highlighted in a recent calculation.[9,10]

Previous studies have also pointed to the importance of Si dangling bonds in driving the nucleation and self-assembly of nanocrystals in a-SiO_2.[32,33] The present results show that low-energy recoils in a-SiO_2 directly produce concentrated pockets of dangling bonds. As described above, O rapidly outdiffuses from damaged regions, leaving regions with high concentrations of Si dangling bonds remaining near the recoil site. These dangling bonds represent highly reactive centers for nanocrystal nucleation, either as Si-rich centers for Si nanocrystal formation, or as chemically active sites for the incorporation of implanted group-IV or metallic ions. These

recoil-induced nucleation sites may explain the rapid nanocrystal formation experimentally observed in the early stages of annealing.[7]

The present results are also applicable to focused electron or ion beam processing of oxides, particularly during nanopore formation.[15,16] Previous studies designed to explore beam-controlled growth and shrinkage of nanometer-scale pores in oxides have observed concentration variations during beam processing associated with preferential O sputtering.[15,34] Existing theories for nanopore formation, particularly with reference to electron irradiation, focus on joule heating and ionization-induced bonding changes as the physical processes driving viscous flow and sputtering of material during irradiation.[16,35] The present results indicate that direct low-energy recoils induced by electron or ion irradiation can play a role both in modifying the bonding network of the target material, and in driving the formation of O-poor regions within the beam spot. In addition, recoil-induced damage to the oxide bonding network may explain electron-beam-enhanced flow under low intensity electron beams.[15,36]

The authors thank Blair Tuttle for providing a-SiO_2 supercells. This work was supported by USAFOSR under MURI Grant No. FA9559-05-1-0306 and the McMinn Endowment at Vanderbilt University.

*m.beck@vanderbilt.edu

[1] S. Tiwari, F. Rana, H. Hanafi, A. Hartstein, E. F. Crabbe, and K. Chan, Appl. Phys. Lett. **68**, 1377 (1996).
[2] L. Pavesi, L. Dal Negro, C. Mazzoleni, G. Franzo, and F. Priolo, Nature (London) **408**, 440 (2000).
[3] L. Ding, T. P. Chen, Y. Liu, M. Yang, J. I. Wong, Y. C. Liu, A. D. Trigg, F. R. Zhu, M. C. Tan, and S. Fung, J. Appl. Phys. **101**, 103525 (2007).
[4] J. Mayandi, T. G. Finstad, S. Foss, A. Thogersen, U. Serincan, and R. Turan, Surf. Coat. Technol. **201**, 8482 (2007).
[5] C. Bonafos *et al.*, J. Appl. Phys. **95**, 5696 (2004).
[6] U. S. Sias, M. Behar, H. Boudinov, and E. C. Moreira, J. Appl. Phys. **102**, 043513 (2007).
[7] B. Garrido Fernandez, M. Lopez, C. Garcia, A. Perez-Rodriguez, J. R. Morante, C. Bonafos, M. Carrada, and A. Claverie, J. Appl. Phys. **91**, 798 (2002).
[8] V. Beyer and J. von Borany, Phys. Rev. B **77**, 014107 (2008).
[9] D. Yu, S. Lee, and G. S. Hwang, J. Appl. Phys. **102**, 084309 (2007).
[10] A. Sarikov, V. Litovchenko, I. Lisovskyy, I. Maidanchuk, and S. Zlobin, Appl. Phys. Lett. **91**, 133109 (2007).
[11] C. J. Nicklaw *et al.*, IEEE Trans. Nucl. Sci. **47**, 2269 (2000).
[12] J. P. Holgado, A. Barranco, F. Yubero, J. P. Espinos, and A. R. Gonzalez-Elipe, Nucl. Instrum. Methods Phys. Res. B **187**, 465 (2002).
[13] W. M. Arnoldbik, N. Tomozeiu, E. D. van Hattum, R. W. Lof, A. M. Vredenberg, and F. H. P. M. Habraken, Phys. Rev. B **71**, 125329 (2005).
[14] S. J. Chang, W. C. Lee, J. Hwang, M. Hong, and J. Kwo, Thin Solid Films **516**, 948 (2008).
[15] A. J. Storm, J. H. Chen, X. S. Ling, H. W. Zandbergen, and C. Dekker, Nature Mater. **2**, 537 (2003).
[16] G. S. Chen, C. B. Boothroyd, and C. J. Humphreys, Appl. Phys. Lett. **62**, 1949 (1993).
[17] M. J. Caturla, T. Diaz de la Rubia, L. A. Marques, and G. H. Gilmer, Phys. Rev. B **54**, 16683 (1996).
[18] K. Nordlund, M. Ghaly, R. S. Averback, M. Caturla, T. Diaz de la Rubia, and J. Tarus, Phys. Rev. B **57**, 7556 (1998).
[19] F. Mota, M. J. Caturla, J. M. Perlado, E. Dominguez, and A. Kubota, Fusion Eng. Des. **75-79**, 1027 (2005).
[20] M. J. Beck, B. R. Tuttle, R. D. Schrimpf, D. M. Fleetwood, and S. T. Pantelides, IEEE Trans. Nucl. Sci. **55**, 3025 (2008).
[21] G. Lucas and L. Pizzagalli, Phys. Rev. B **72**, 161202(R) (2005).
[22] W. Windl, T. J. Lenosky, J. D. Kress, and A. F. Voter, Nucl. Instrum. Methods Phys. Res. B **141**, 61 (1998).
[23] E. Holmström, A. Kuronen, and K. Nordlund, Phys. Rev. B **78**, 045202 (2008).
[24] M. J. Beck, R. D. Schrimpf, D. M. Fleetwood, and S. T. Pantelides, Phys. Rev. Lett. **100**, 185502 (2008).
[25] K. O. Ng and D. Vanderbilt, Phys. Rev. B **59**, 10132 (1999).
[26] Y. Tu and J. Tersoff, Phys. Rev. Lett. **84**, 4393 (2000).
[27] J. P. Perdew and A. Zunger, Phys. Rev. B **23**, 5048 (1981).
[28] D. Vanderbilt, Phys. Rev. B **41**, 7892 (1990).
[29] J. M. Pruneda and E. Artacho, Phys. Rev. B **70**, 035106 (2004).
[30] C. Levelut, A. Faivre, R. Le Parc, B. Champagnon, J. L. Hazemann, and J. P. Simon, Phys. Rev. B **72**, 224201 (2005).
[31] Y. G. Jin and K. J. Chang, Phys. Rev. Lett. **86**, 1793 (2001).
[32] A. Losavio, B. Crivelli, F. Cazzaniga, M. Martini, G. Spinolo, and A. Vedda, Appl. Phys. Lett. **74**, 2453 (1999).
[33] Y. Liu, T. P. Chen, Y. Q. Fu, M. S. Tse, J. H. Hsieh, P. F. Ho, and Y. C. Liu, J. Phys. D **36**, L97 (2003).
[34] M. Y. Wu, D. Krapf, M. Zandbergen, H. Zandbergen, and P. E. Batson, Appl. Phys. Lett. **87**, 113106 (2005).
[35] W. M. Zhang, Y. G. Wang, J. Li, J. M. Xue, H. Ji, Q. Ouyang, J. Xu, and Y. Zhang, Appl. Phys. Lett. **90**, 163102 (2007).
[36] F. Sola, O. Resto, A. Biaggi-Labiosa, and L. F. Fonseca, Nanotechnology **18**, 405308 (2007).